Title

Aeolian dust deposition and the perturbation of phosphorus transformations during long-term ecosystem development in a cool, semi-arid environment

Authors

Gu, Chunhao
Hart, Stephen C
Turner, Benjamin L
et al.

Publication Date

2019-02-01

DOI

10.1016/j.gca.2018.12.017

Peer reviewed

Available online at www.sciencedirect.com

ScienceDirect

Geochimica et Cosmochimica Acta 246 (2019) 498–514

Geochimica et Cosmochimica Acta

www.elsevier.com/locate/gca

Aeolian dust deposition and the perturbation of phosphorus transformations during long-term ecosystem development in a cool, semi-arid environment

Chunhao Gu [a], Stephen C. Hart [b], Benjamin L. Turner [c], Yongfeng Hu [d], Yong Meng [e], Mengqiang Zhu [a,*]

[a] Department of Ecosystem Science and Management, University of Wyoming, Laramie, WY 82071, United States
[b] Department of Life & Environmental Sciences and Sierra Nevada Research Institute, University of California, Merced, CA 95343, United States
[c] Smithsonian Tropical Research Institute, Apartado 0843-03092, Balboa, Ancon, Panama
[d] Canadian Light Source, University of Saskatchewan, Saskatoon S7N 2V3, Canada
[e] State Key Laboratory of Ore Deposit Geochemistry, Institute of Geochemistry, Chinese Academy of Sciences, Guiyang 550002, Guizhou, China

Received 13 March 2018; accepted in revised form 13 December 2018; Available online 19 December 2018

Abstract

Aeolian dust deposition is an important phosphorus (P) input to terrestrial ecosystems, but its influence on P dynamics during long-term ecosystem development remains poorly understood. In this study, we characterized P speciation using P K-edge XANES spectroscopy in surface soils (0–15 cm, A horizon) and contemporary aeolian dust collected at each site of a 3000-ky volcanic soil chronosequence in a cool, semi-arid environment. Phosphorus speciation in dust was dominated by calcium-bound P (Ca-P; 54–74%), with 11–23% iron and aluminum-bound P [(Fe + Al)-P] and 7–25% organic P (P_o). In soils, P_o contributed 1–23% of total P, being greater in older soils; however, the proportions of Ca-P (16–39%) and (Fe + Al)-P (48–82%) fluctuated with increasing weathering over the soil chronosequence. These soil fluctuations resulted from the accumulation and preservation of alkaline aeolian dust during pedogenesis in the semi-arid climate, which significantly increased soil Ca-P while decreasing the total amounts and relative abundances of soil (Fe + Al)-P. We suggest that the effects of an aeolian dust input on soil P transformations are functions of the relative magnitude and chemical composition of the dust input and the soil weathering intensity. For a given source of dust, when the net dust flux is greater than the weathering rate, dust accumulates and thus alters the pattern of P transformations during pedogenesis; otherwise, the dust influence on soil P transformations is negligible. By accurately identifying the chemical nature of P pools, our work highlights the advantage of P K-edge XANES spectroscopy over chemical extractions in examining soil P dynamics, and demonstrates how dust inputs can modify the Walker and Syers model of pedogenic P transformations in semi-arid environments. Overall, this work provides a foundation for understanding how dust influences P cycling during soil and ecosystem development, and indicates that dust inputs and composition, and the soil weathering rate, all must be considered for developing integrated climate-biogeochemical models with predictive power in terrestrial ecosystems.
Published by Elsevier Ltd.

Keywords: Phosphorus transformations; Soil development; Aeolian dust inputs; P K-edge X-ray absorption spectroscopy

1. INTRODUCTION

Phosphorus (P) is an important nutritional element that often limits terrestrial ecosystem productivity and

* Corresponding author.
E-mail address: mzhu6@uwyo.edu (M. Zhu).

https://doi.org/10.1016/j.gca.2018.12.017
0016-7037/Published by Elsevier Ltd.

decomposition, and influences carbon (C) and nitrogen (N) cycling in soils (Elser et al., 2007; Selmants and Hart, 2010; Wang et al., 2015). Soil P is derived ultimately from rock weathering, so pedogenesis strongly determines the stock, speciation (i.e., the distribution of P as different chemical species) and bioavailability of P in terrestrial ecosystems (Walker and Syers, 1976). At a given stage of pedogenesis, P speciation provides a useful context for evaluating contemporary cycling of P and other nutrients, and for determining how changes in P availability might affect ecosystem processes (Ceulemans et al., 2017; Crews et al., 1995; Wardle et al., 2004; Zemunik et al., 2015). However, P transformations during pedogenesis in semi-arid ecosystems remain unclear and the effects of aeolian dust inputs to soils are poorly understood.

Phosphorus transformations during pedogenesis have been described by the conceptual model proposed by Walker and Syers (1976, Fig. 1a). In the Walker and Syers model, soil pH declines during pedogenesis, dissolving the primary P-bearing minerals (i.e., apatite) and releasing soluble P to soil solution. The soluble P is lost via leaching and runoff, assimilated by biota to form organic P (P_o), or adsorbed/precipitated on the surfaces of newly-formed secondary minerals including iron (Fe) and aluminum (Al) oxides and phyllosilicates. The soluble P may precipitate as calcium (Ca) phosphates, and probably also Fe and Al phosphates although not very often detected. The soluble and weakly sorbed P together are termed "non-occluded" P ($P_{n\text{-}occ}$) and have the highest bioavailability among the four pools, while occluded P (P_{occ}) that is P strongly bound to Al and Fe or physically protected is the least bioavailable. In late stages of soil development, the soil P pool is dominated by both P_o and P_{occ}. A recent study determined the turnover time of these pools (Helfenstein et al., 2018). In addition to soluble P loss from leaching and runoff, total soil P continues to decline during soil development because of surface erosion (Aciego et al., 2017; Arvin et al., 2017).

Using soil chronosequences and P chemical extractions, a number of studies have shown that the Walker and Syers model accurately describes P transformations in humid ecosystems (Crews et al., 1995; Lichter, 1998; Parfitt et al., 2005; Prietzel et al., 2013; Turner and Laliberté, 2015; Vitousek and Farrington, 1997; Walker and Syers, 1976). However, in semi-arid and arid environments, only three previous studies tested the model and conclusions were inconsistent. The P pools changed systematically as predicated by the Walker and Syers model in Selmants and Hart (2010) using a soil chronosequence derived from basaltic cinders, but not in Lajtha and Schlesinger (1988) and Meixner and Singer (1985). It therefore remains unclear whether the Walker and Syers model is applicable to more arid ecosystems.

Aeolian dust deposition is a ubiquitous P input to ecosystems that can affect soil chemistry, mineralogy, and nutrient status, even at remote sites far from terrestrial dust sources (Chadwick et al., 1999; Kurtz et al., 2001; Lawrence et al., 2013; Muhs and Benedict, 2006; Porder et al., 2007; Simonson, 1995). Mineral dust generated from drylands is typically alkaline and calcareous (Hou et al., 2018;

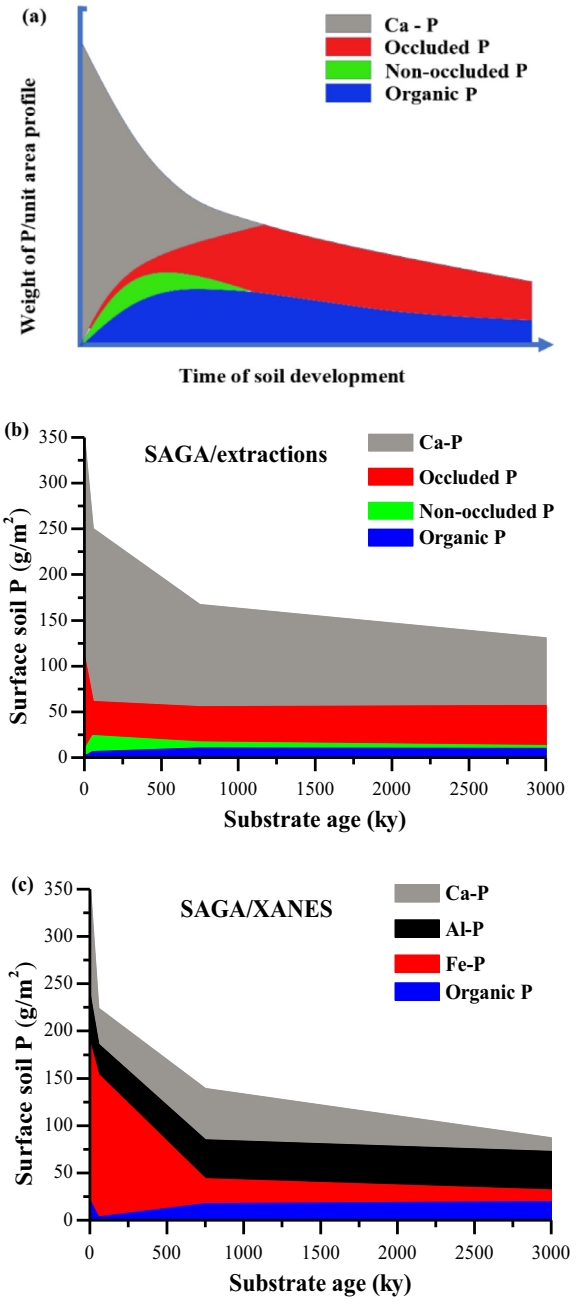

Fig. 1. (a) Phosphorus (P) transformations during pedogenesis described using the Walker and Syers model assuming no significant external disturbance, such as dust input during soil development; (b) changes of the P pools of the Walker and Syers model in the surface soils (0–15 cm) during soil development across the substrate age gradient of Arizona (SAGA) as measured by the modified Hedley chemical sequential extractions. These data were reported previously in Selmants and Hart (2010); and (c) The XANES-determined P speciation changes in these soils in the present study. The total P concentrations in (b) and (c) were measured respectively in Selmants and Hart (2010) and in the present study, so the values at each substrate age were slightly different.

Hudson-Edwards et al., 2014; Zhang et al., 2018) although not always (Wagenbach and Geis, 1989) and can therefore increase soil pH (Sauer et al., 2007). Due to input of new parent materials and elevated pH, chemical weathering can be retarded (Sauer et al., 2007). However, aeolian dust deposition has also been hypothesized to enhance soil physical and chemical weathering by promoting water holding capacity due to the deposition of the fine dust particles (Rasmussen et al., 2017). Thus, it is critical to understand how dust deposition affects the soil weathering and nutrient cycling of ecosystems where dust inputs are significant.

The dust contribution to soils and nutrient status increases with substrate age because of continuous dust deposition (Chadwick et al., 1999). This in turn can influence patterns of elemental composition and mineralogy of soils during pedogenesis (Muhs, 2001; Sauer et al., 2007), and thus affect P transformations. However, few studies of P transformations consider dust inputs, presumably because it is difficult to calculate historical inputs during the lifespan of the chronosequence, even though dust inputs can sometimes account for the majority of the mass of old soils (Coble et al., 2015; Selmants and Hart, 2010). Aeolian dust input was assumed to be negligible in the soils of the chronosequences in New Zealand used to propose the Walker and Syers model, although a later study shows that the oldest stages of one of the chronosequences (the Franz Josef sequence) have received considerable dust input during glacial cycles when loess inputs were considerable (Almond et al., 2001). Crews et al. (1995) suggested that aeolian dust inputs maintained available P during long-term soil development in the humid tropical Hawaiian Islands, which was supported later by Chadwick et al. (1999). Eger et al. (2012, 2013a, 2013b) considered the fate of P in aeolian dust deposited to a super-humid, temperate environment and found that acidic organic surface soil layers assimilated dust-borne calcium-bound P (Ca-P), providing soluble P that can enlarge P_o and Fe- and Al-P pools.

Understanding the impact of dust inputs on soil P transformations during pedogenesis requires accurate information on soil P speciation that ultimately controls the fate, behavior, and bioavailability of soil P. Sequential chemical extractions, such as the Hedley fractionation scheme and its modified versions, have been widely used to classify soil P into various pools of different bioavailability, and have been used to test the Walker and Syers model (e.g., Crews et al., 1995; Cross and Schlesinger, 2001; Selmants and Hart, 2010). Sequential P fractionation schemes potentially provide rich information about P pools, but this information might be misleading because each P pool is operationally defined and does not necessarily correspond to a definite P species (Condron and Newman, 2011; Kar et al., 2011; Negassa and Leinweber, 2009; Zhang et al., 2018). In addition, the extraction is destructive and may affect the results of the next sequential extraction step (Barbanti et al., 1994; Condron and Newman, 2011; Houhou et al., 2009). Because of the disadvantages of the methods used to define the conceptual pools, the Walker and Syers model is inherently limited in its capability to describe P transformations without the results of the methods being tied unambiguously to soil P composition.

Phosphorus K-edge X-ray absorption near-edge structure (XANES) spectroscopy is a direct and non-invasive technique for soil P speciation characterization (Giguet-Covex et al., 2013; Hesterberg et al., 1999; Kizewski et al., 2011; Kruse and Leinweber, 2008; Prietzel et al., 2013; Shober et al., 2006; Wu et al., 2014; Zhang et al., 2018). It divides P speciation into four main categories: Ca-P, Fe-P and Al-P that are inorganic phosphate, and P_o. Each category could contain more than one specific P species, as different species in the same category have similar spectral feature and cannot be confidently differentiated (Ajiboye et al., 2008; Prietzel et al., 2016). XANES spectroscopy provides much more accurate information about inorganic P speciation than other currently available methods (Zhang et al., 2018), although quantification of each P category has a degree of uncertainties due to the artifacts introduced during XANES data processing, the types of the reference spectra selected for the XANES linear combination fitting (LCF) analysis, and the relatively poor spectral quality. In addition, XANES spectroscopy is unable to identify different organic P species in soils and ^{31}P nuclear magnetic resonance spectroscopy is more powerful (Kruse et al., 2015). Only one study has applied this technique to examine changes in P speciation during pedogenesis. Prietzel et al. (2013) used P K-edge XANES spectroscopy and observed rapid changes in P speciation in the surface soils of two glacier foreland chronosequences up to 700 y in humid climates. Based on the XANES analysis, they concluded that the Walker and Syers model can describe short-term changes of P speciation in proglacial surface soils (Prietzel et al., 2013).

The aim of the present study was to determine how dust deposition affects the pattern of soil P transformations during long-term ecosystem development in a cool, semi-arid climate. We determined P speciation in surface soil and contemporary dust samples collected at each site of a 3000-ky semi-arid volcanic soil chronosequence using P K-edge XANES spectroscopy. Elemental and mineral composition of soil and dust samples were characterized to determine dust impacts on soil chemistry and mineralogy. Based on our data, we propose a new conceptual model suggesting that the influence of dust on soil P transformations during soil development depends on the interactions between the magnitude and composition of dust inputs and the rate of soil weathering.

2. MATERIALS AND METHODS

2.1. Study sites

Soil samples were collected from four sites of different substrate ages located in the San Francisco Volcanic Field in northern Arizona, United States, which form the Substrate Age Gradient of Arizona (SAGA; Fig. A1 of the Electronic Annex). The sites differred markedly in the substrate ages (i.e., 1 ky, 55 ky, 750 ky and 3000 ky), but had similar contemporary climate (a cool, semi-arid climate with mean annual temperature 11 °C and mean annual precipitation 340 mm), vegetation, topography (elevation ~2000 m with slopes <1%), and parent material (micropor-

phyritic basalt scoria). The vegetation was co-dominated by piñon pine, *Pinus edulis,* and one-seed juniper, *Juniperus monosperma.* The inter-canopy space was covered by primarily the C4 perennial bunchgrass blue gramma (*Bouteloua gracilis*) for the three older sites, while the inter-canopy at the youngest site was sparsely vegetated with woody shrubs, primarily *Fallugia paradoxa* and *Rhus trilobata.* These four sites form a well-constrained, model system for studying ecology and biogeochemical cycles during ecosystem development in a semi-arid environment (Coble and Hart, 2013, 2016; Coble et al., 2015; Newman and Hart, 2015; Selmants and Hart, 2010).

2.2. Soil and dust sampling

The soil and dust samples from the SAGA sites in the present study were the same as those in the previous studies that examined C and N dynamics, nutrient limitation, and effects of dust inputs on nutrient supply (Coble et al., 2015; Selmants and Hart, 2008, 2010). These soils were also studied for P transformations using the modified Hedely sequential chemical extraction scheme and the pools were found to be consistent with the Walker and Syers model (Selmants and Hart, 2010; Fig. 1b). All the samples were collected with a 1.9-cm diameter Oakfield soil sampler. Eight surface mineral soil samples (0–15 cm, A horizon) were obtained from eight inter-canopy spaces (minimum of 10-m in diameter between trees) at each site, and each of the eight samples was a composite of six subsamples. The A horizon was chosen for study because it is the initial recipient of aeolian dust inputs (the inter-canopy spaces have little to no surficial organic horizon). Hence, we expected the interactions between dust inputs and soil weathering processes to be maximal within this soil horizon.

After air drying and sieving (<2 mm), the eight samples were further pooled to make one composite sample per site, resulting in totally four composite samples of different substrate ages across the chronosequence. All characterizations in this study were based on the composite samples and reported errors were analytical errors rather than field variability. Site-composite soil samples were used because the available beamtime of XANES measurements precluded within-site replication of soil analyses, and measurements of contemporary dust inputs were unreplicated at the inter-canopy space (i.e., plot) scale (see below). Previous studies using these soils have shown that within-site variation in soil elemental pools and transformation rates were much lower than among-site variation based on analyzing soils from these same eight inter-canopy spaces per site (Coble and Hart, 2013; Coble et al., 2015; Selmants and Hart, 2008, 2010). Thus, we assume that the within-site variations of the data obtained in the present study were also significantly smaller than the variation in the same fractions across the four site.

Sieved samples were stored under dark and dry conditions to minimize changes caused by storage. A small fraction of each composite sample was finely ground using a ball mill to pass through 100-mesh sieve (<0.15 mm) for all analyses in the present study. Carbonate was not detected in the soils at any of the four sites (Selmants and Hart, 2008).

Using strontium (Sr) isotope techniques, Coble et al. (2015) showed that the dust mass contribution to soils (to a 2-m depth) across SAGA increased from 2% at the 1-ky site to 100% at the 3000-ky site (also in Table 1). The contemporary annual dust flux was 3.5–11.3 g m^{-2} y^{-1} based on mass of dust collected per trap over time. Dust samples were collected over a one-year period at each site using three passive dust collectors (area of collector was 0.066 m^2) placed on a pole 2 m above the ground within inter-canopy spaces (Coble et al., 2015). Large (>0.5 mm) organic detritus in the samples were removed from the dust samples using forceps and a dissecting microscope. More details about dust collection are provided in Coble et al. (2015). Contemporary dust inputs appear to originate from the Mojave and Sonoran deserts, with some contributions from the Colorado Plateau to the east and north (Rasmussen et al., 2017). Asian dust sources may also contribute to the total dust inputs at these sites based on comparative Sr isotope values of collected dust and Asian soil samples, and Hysplit back trajectory model runs for the dust collection period (Coble et al., 2015).

Table 1
Chemical Index of Alteration (CIA) and total K/Na molar ratios for the soil and dust samples (one composite sample per site) at each chronosequence site. Dust contributions to soil mass based on Sr isotope composition reported in Coble et al. (2015) and soil pH data reported in Selmants and Hart (2008) are included here to assist in data interpretation. The mean and standard errors (in parentheses) for soil pH are based on eight surface mineral soil (0–15 cm) samples taken from eight inter-canopy spaces at each site. Dust contributions to soil are based on dust inputs to passive collectors placed on 2-m poles at each site (n = 3 collectors per site).

	Substrate Age (ky)	pH	K/Na molar ratio	CIA	Dust Contribution (%) based on Sr isotope	Dust Contribution (%) based on quartz contents
Soil	1	6.74 (0.15)	0.17	58.9	2 (3)	17 (2)
	55	6.56 (0.04)	0.45	66.4	24 (7)	40 (3)
	750	6.70 (0.13)	0.86	68.7	54 (29)	82 (6)
	3000	6.17 (0.06)	1.25	70.4	>100 (0)	103 (7)
Dust	1	–	0.59	52.8	–	–
	55	–	0.50	59.3	–	–
	750	–	0.79	51.5	–	–
	3000	–	0.88	79.6	–	–

2.3. Determination of soil and dust chemical properties

2.3.1. Total elemental concentrations

Ground soil subsamples were made into fused beads for determination of major element concentrations. A PANalytical Axios X-Ray Fluorescence (XRF) analyzer equipped with a 4000 W Rh SST-max X-ray tube and three wavelength-dispersive spectrometers was used to quantify the total concentration of major elements. The NIST reference soils (2704 Buffalo River Sediment, 2709 San Joaquin Soil, and 2710a Montana Soil I and II) and duplicate measurements indicate the relative standard deviation of the composition measurement was <8%. The elemental composition in dust was measured by digestion with hydrogen fluoride. The concentrations of the dissolved elements were measured using inductively coupled plasma atomic emission spectroscopy (ICP-AES). The relative standard errors for the ICP-AES analysis were below 3% for all samples.

2.3.2. Pedogenic Al and Fe

The pedogenic Fe and Al were separated into oxalate- and dithionite-extractable pools. The two pools were extracted sequentially, rather than on two different subsamples (Miller et al., 2001). The ammonium oxalate solution of pH 3 (Sparks et al., 1996) was used to extract Fe and Al (Al_{ox} and Fe_{ox}) in poorly crystalline minerals (e.g., ferrihydrite, allophane and imogolite) and bound to soil organic matter from the soils (Parfitt and Henmi, 1982). The non-crystalline Al-bearing minerals in basalt parent materials were also extractable by the oxalate extractions (Selmants and Hart, 2010). About 0.5 g soil or 0.05 g dust was added to 30 ml of pH 3.0 ammonium oxalate solution in a 50-ml polypropylene centrifuge tube. The suspension was agitated for 2 hours under dark condition on a reciprocal shaker. The supernatants were collected by centrifuge and the solid residue of the oxalate extraction was then extracted with 30-ml dithionite-citrate solution to determine the contents of well-crystallized Fe oxides (Fe_{di}) including Al (Al_{di}) incorporated into the structure of the Fe oxides. The 30-ml dithionite-citrate solution contained 0.5 g $Na_2S_2O_4$ and 6 g $Na_3C_6H_5O_7{\cdot}2H_2O$. The suspension was agitated overnight (16 h) on a reciprocal shaker. The Fe, Al and P concentrations in both oxalate and dithionite extracts were measured using ICP-AES. As the two pools were extracted sequentially, the sum of the oxalate and dithionate extracted Fe and Al represented the total contents (Fe_{ox+di} and Al_{ox+di}) of pedogenic Fe and Al. Phosphorus (P_{di} and P_{ox}) associated with Fe and Al was also extracted by the above processes. One of the soil samples were conducted in triplicates to estimate the analytical uncertainties of the extractions and the relative standard error was determined to be within 4%.

2.3.3. Weathering indices

The oxalate extracted Al (Al_{ox}) (see Section 2.3.2), Chemical Index of Alteration (CIA), and the K/Na molar ratio were adopted as proxies to estimate the degree of weathering across the substrate age gradient. Although CIA may not be applicable to semi-arid soils due to limited leaching (Frey et al., 2013), CIA generally reflects the degree of the transformation from primary mineral feldspars to secondary clay minerals during pedogenesis (Nesbitt and Young, 1982). The CIA was calculated using the following formula (Nesbitt and Young, 1982):

$$\mathrm{CIA} = 100\frac{\mathrm{Al_2O_3}}{\mathrm{Al_2O_3} + \mathrm{CaO^*} + \mathrm{K_2O} + \mathrm{Na_2O}}$$

where CaO^* represents the Ca content in silicate minerals (McLennan, 1993). To exclude interference from the Ca associated with carbonates, phosphates and sulfates, the mole value of CaO^* was assumed to be equal to that of Na_2O when the CaO mole number is larger than that of Na_2O; otherwise, the measured CaO value was used (McLennan, 1993).

2.4. Mineralogy of soils and dust

X-ray diffraction (XRD) was used to identify and quantify the minerals in the soil and dust samples. The XRD data were collected at the Advanced Photon Source, Argonne National Laboratory using X-rays of 58.649 keV ($\lambda = 0.2115$ Å) with a sample-to-detector distance of ~95 cm and an amorphous silicon image plate at beamline 11-ID-B. Each ground sample was packed into a Kapton capillary tubing with an inner diameter of ~1 mm for the measurements. Diffraction data of an empty Kapton tubing were measured as the background, which was subtracted from the sample data. The 2-D images of the raw data were integrated and converted to 1-D intensity versus wave vector (Q) using the Fit2D program (Hammersley, 1998). Calibration of the sample-to-detector distance, beam center position, and tilt angles of the detector relative to the beam path was conducted using the standard CeO_2 available at the beamline. The diffraction data were then converted to 2θ with Cu K_α radiation ($\lambda = 1.5406$ Å) for quantitative XRD analysis (see below). The detection limit of the synchrotron-based X-ray diffraction analysis is ~0.3% (Leon-Reina et al., 2016).

The MDI Jade 6.0 software (Livermore, CA, USA) was used to identify and quantify the mineral phase in the samples. The identification was conducted through comparing the XRD pattern of the sample with standard patterns of the possible phases from the International Centre for Diffraction Data (ICDD). The percentages of major components were modeled by the whole pattern fitting (WPF) refinement with the JADE 6 program (da Silva et al., 2017). The inclusion of whole XRD patterns in the fittings takes background, crystallinity, and preferred orientation into account in the fittings (Chipera and Bish, 2013), which gives rise to more reliable results compared with traditional reference intensity ratio (RIR) analysis (Hubbard and Snyder, 1988). In addition, the WPF refinement can be applied without the addition of an internal standard (Chipera and Bish, 2013).

2.5. Phosphorus K-edge XANES Spectroscopy

Phosphorus speciation in the soil and dust samples were determined using LCF analysis of P K-edge XANES spectra with a pool of P reference spectra (Giguet-Covex et al.,

2013; Hesterberg et al., 1999; Hou et al., 2018; Hudson-Edwards et al., 2014; Prietzel et al., 2013). Three P compounds used in the XANES LCF analysis were purchased from Sigma-Aldrich: sodium phytate to represent P_o, and hydroxyl apatite (HAP) and calcium dihydrogen phosphate monohydrate [$Ca(H_2PO_4)_2{\cdot}H_2O$] to represent the primary Ca-P mineral and secondary Ca-P minerals, respectively. The Fe-P reference used in the LCF was phosphate adsorbed on ferrihydrite and the Al-P references included phosphate adsorbed on amorphous Al oxides and kaolinite. The kaolinite was purchased from the Source Clays Repository of the Clay Minerals Society (Purdue University, West Lafayette, Indiana, USA). The ferrihydrite and amorphous Al oxides were synthesized according to the methods in Gu et al. (2016) and Yan et al. (2014). The adsorption experiments were conducted by reacting 5 mM phosphate with 2 g L^{-1} two-line ferrihydrite or amorphous Al hydroxides or kaolinite in 0.1 M $NaNO_3$ at pH 5.5 for 3 days at room temperature (~21 °C). The samples were then filtered and air-dried at room temperature for 24 hours prior to P K-edge XANES data collection. For both Fe-P and Al-P references, amorphous Fe and Al phosphates may form as a result of phosphate adsorption on the two metal oxides (Wang et al., 2017), and thus, the Fe-P and Al-P reference spectra did not only represent surface-adsorbed phosphate. These P reference compounds represent the major P species in soils and dust and similar reference compounds have been used previously (Giguet-Covex et al., 2013; Hesterberg et al., 1999; Kizewski et al., 2011; Kruse and Leinweber, 2008; Prietzel et al., 2013; Prietzel et al., 2016; Shober et al., 2006; Wu et al., 2014; Zhang et al., 2018).

Phosphorus K-edge XANES spectra were collected from the P references and the soil and dust samples at the Soft X-ray Micro Characterization Beamline (SXRMB) at the Canadian Light Source (CLS), Saskatoon, Canada. The beamline was equipped with a Si (1 1 1) double-crystal monochromator and a Si drift fluorescence detector, covering an energy range from 1.7 to 10 keV. Each finely ground sample was spread as thin film on a double-sided P-free carbon tape that was adhered to a copper stick for the XANES data collection. The sample chamber was in vacuum to reduce beam attenuation by air. All samples and the two P adsorption references were measured in fluorescence mode, while the other four reference compounds were measured in total electron yield (TEY) mode to avoid self-absorption. The step size was 2 eV in the pre-edge region (2110–2140 eV), 0.15 eV at the edge step (2140–2175 eV), and 0.75 eV in the post-edge region (2175–2210 eV) using a dwell time of 4 s for the samples and the two adsorption references, and 1 s for the other four reference compounds. Two or more scans of each specimen were collected and averaged to improve data quality. The repeated measurements for each sample indicate that the spectra were reproducible, suggesting no radiation damage of the samples. The program SIXPack (Webb et al., 2005) was used to average the scans. The Athena program was used (Ravel and Newville, 2005) for background removal (energy range: 2125–2140 eV), normalization (2174–2210 eV), and LCF analysis (2140–2190 eV). The LCF analysis allowed the relative quantification of each P species in the dust and soil samples. Energy shifts were not allowed during the LCF analysis. The LCF analysis was performed for all possible combinations of the reference spectra. The goodness-of-fit was indicated by the R-factor. The error of the XANES LCF analysis is difficult to quantify; as a rule of thumb, the absolute error is ~10%, (Ajiboye et al., 2008; Helfenstein et al., 2018; Prietzel et al., 2016; Werner and Prietzel, 2015).

3. RESULTS

3.1. Soil and dust chemical properties

As reported previously, soil morphology and physical properties exhibited important correlations with substrate age. For instance, the thickness of the soil solum and clay content both increased with increasing substrate age (Coble et al., 2015; Selmants and Hart, 2008, 2010). In addition, soil pH values (determined in 1:2 mass of air-dry soil to volume of 0.01 M $CaCl_2$ suspensions; Selmants and Hart, 2008) declined from 6.74 at the 1-ky site to 6.17 at the 3000-ky site, except the abnormally high value (pH = 6.70) at the 750-ky site (Table 1). The weakly acidic soil pH is consistent with the absence of carbonates and suggests that appreciable leaching still occurs (Dahlgren et al., 1997), as discussed below.

The elemental composition of the surface soils also changed with substrate age. With increasing age, Si, K and Zr concentrations all increased, while P, Al, Fe, Mn, Mg, Ca and Na concentrations all decreased (Table 2). The Ti concentration slightly decreased with substrate age except for the high value at the 750-ky site. Leaching of mobile elements was evaluated based on the concentration ratios of elements to the relatively immobile element Ti. Ti was chosen rather than Zr because Zr in soils was associated with quartz input from dust but Ti was relatively unaffected by dust inputs (Heckman and Rasmussen, 2011). This is also corroborated by the 4-fold increase in the Zr concentration in soils with increasing substrate age (Table 1), as the older sites received more dust inputs. The mass ratios of P_2O_5, Fe_2O_3, Na_2O, CaO and MgO to TiO_2 all decreased with substrate age, whereas the K_2O/TiO_2 ratio increased and the Al_2O_3/TiO_2 ratio fluctuated with increasing substrate age (Fig. 2a–c). The SiO_2/Al_2O_3 ratio increased with increasing substrate age (Fig. 2d). The CIA value (58.9–70.4) and the K/Na ratio (0.17–1.25) both increased with increasing substrate age (Table 1).

The same set of elements as in the soil were measured for the dust samples, except Si and Ti (Table 2). Majority of the measured elements had lower concentrations in the dust than in the soil at each site. The CIA values and the K/Na ratios for the dust samples were 0.59–0.88 and 51.5–79.6, respectively.

3.2. Pedogenic Fe and Al in soil and dust

With increasing substrate age, the Fe_{ox} concentration in the surface soils increased slightly from 15 g/kg at the 1-ky site to 17.5 g/kg at the 55-ky site, and then dropped sharply to ~2.5 g/kg at the two older sites (Fig. 3a). These corre-

Table 2
Total elemental concentrations in surface soil (0–15 cm) and dust. All concentration data are in weight percentage (%) oven-dry material except for Zr in mg/kg. Si and Ti were not measured for the dust.

Age (ky)	Si	Ti	Al	Fe	Mn	Mg	Ca	Na	K	P	Zr
Soil											
1	21.9	1.1	8.2	8.5	0.14	5.4	6.6	2.3	0.7	0.18	8.9
55	24.5	0.8	8.0	6.6	0.13	3.3	4.0	1.4	1.1	0.13	17.8
750	25.5	0.9	7.7	5.9	0.12	1.2	2.2	1.1	1.5	0.09	22.9
3000	28.7	0.7	7.0	4.7	0.12	1.2	1.3	0.8	1.6	0.05	37.0
Dust											
1	–	–	3.6	2.2	0.04	0.06	1.71	1.06	1.06	0.09	100.1
55	–	–	4.4	2.6	0.05	0.08	2.16	1.03	0.88	0.10	107.9
750	–	–	4.2	2.4	0.05	0.07	2.49	1.21	1.62	0.18	157.6
3000	–	–	11.3	8.1	0.14	0.23	3.23	0.86	1.28	0.04	191.0

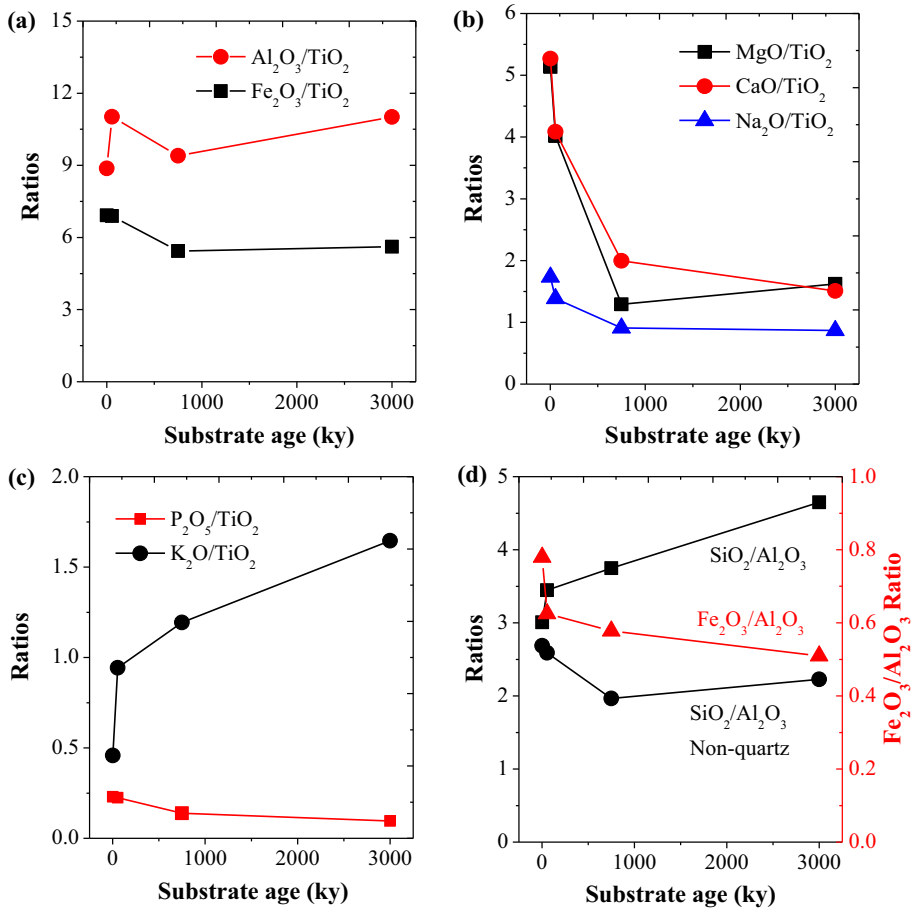

Fig. 2. Mass ratios of P_2O_5, Fe_2O_3, Al_2O_3, MgO, CaO, Na_2O, P_2O_5 and K_2O to TiO_2 (a–c) and molar ratios of Fe_2O_3, SiO_2, and SiO_2 (non-quartz) to Al_2O_3 (d) for surface soils (0–15 cm) across the substrate age gradient, shown as a function of substrate age. In (d), the non-quartz associated Si was calculated by subtracting the amount of Si in quartz (estimated by XRD) from the total SiO_2 content. The uncertainties of the data points were estimated to be ~4% and represent analytical errors from composite samples.

spond to 20–27.5% of the total Fe for the younger soils and ~5% for the older ones (Fig. 3b). The proportion of Fe_{di} to the total Fe increased from 12.0% to 22.8% with increasing substrate age (Fig. 3d). The two younger soils had similar Fe_{ox+di} (~23 g/kg), which decreased to 12.5 g/kg at the two older sites (Fig. 3e). The proportion of Fe_{ox+di} to the total Fe increased from 30.6% for the 1-ky site to 39.3% for the 55-ky site, and then decreased to about 25% for the two older sites (Fig. 3f).

The Al_{ox} concentration decreased monotonically from 8.1 to 3.4 g/kg with increasing substrate age (Fig. 3a), corresponding to 9.3–5.1% of total Al. The Al_{ox} concentration was much lower than the Fe_{ox} concentration for the two younger soils, while slightly higher than the Fe_{ox} concentra-

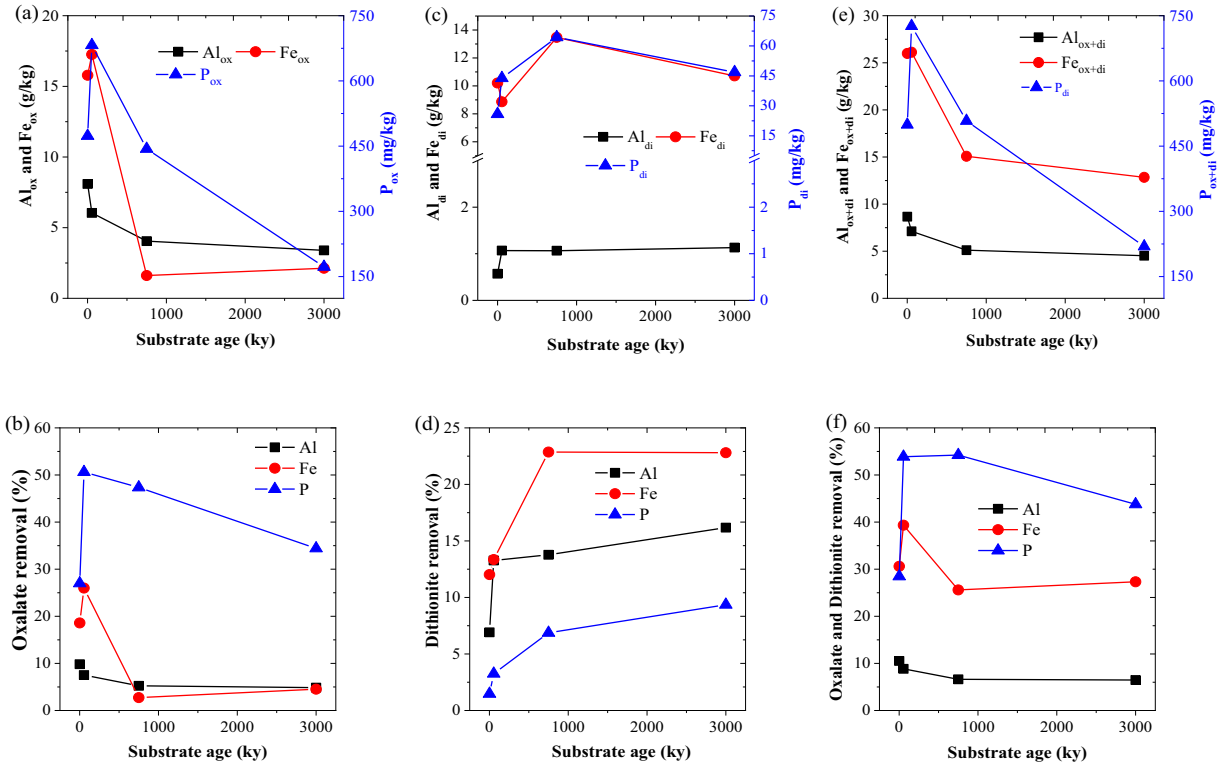

Fig. 3. Concentrations of oxalate and dithionite extractable Fe, Al, and P (a, c, e) and percentages of their removals (% of total concentration; b, d, f) from surface soils (0–15 cm) across the substrate age gradient. The scale is different for P in a, c and e. The uncertainties of the data points were estimated to be ~4% and represent analytical errors from composite samples.

tion for the two older soils (Fig. 3a). Al_{ox+di} was only slightly higher than Al_{ox} (Fig. 3d) because dithionite did not dissolve crystalline Al-bearing minerals, such as gibbsite and kaolinite (Sparks et al., 1996). The dissolution of Fe- and Al-bearing minerals during oxalate and dithoinite extractions led to release of associated P. The P_{ox} concentration and proportion to soil total P both increased and then decreased across the soil chronosequence (Fig. 3a and b), similar to the changes in Fe_{ox} (Fig. 3a). Dithionite removed increasingly more P (P_{di}) with increasing substrate age (Fig. 3d).

Dust collected at each site also contained pedogenic Fe and Al, as shown in Table 3. The Fe_{ox} and Fe_{di} concentrations were 3.1–5.1 g/kg and 5.9–7.8 g/kg, respectively, accounting for 5.2–19.6% and 8.7–30.7% of the total Fe. Together, oxalate and dithionite extracted 13.9–49.8% of total Fe. Al_{ox} (1.8–2.3 g/kg), Al_{di} (1.2–1.4 g/kg) and Al_{ox+di} (3.0–3.6 g/kg) all had significantly lower concentrations than the corresponding extracted Fe.

3.3. Mineralogy of soil and dust

The mineralogy of the surface soils and dust samples were characterized using quantitative XRD analysis (Table 4). The XRD patterns are provided in Fig. A2 of the Electronic Annex. The soils contained anorthite (plagioclase feldspar) and augite (pyroxene), which decreased with increasing substrate age from 58% to 25% and from 21% to 0% in weight percentages, respectively. Olivine was detected only at the youngest site, consistent with its fast weathering. The concentration of quartz increased from 5% to 32% with increasing substrate age. Muscovite was absent in the 1-ky old soils, and its proportion ranged from 44% to 38% for the three older soils. In addition, hematite was found at

Table 3
Concentrations (g/kg) and percentages (in parentheses, % of total Fe or Al concentration) of the pedogenic Fe and Al in dust (one composite sample per site). Ox: oxalate extractable; Di; dithionite-citrate extractable elements in the residue of the oxalate extraction. Fe_{ox+di} and Al_{ox+di} are the sum of the oxalate extractable and dithionite-citrate extractable Fe and Al, respectively.

Age (ky) of dust collection site	Fe_{ox}	Fe_{di}	Fe_{ox+di}	Al_{ox}	Al_{di}	Al_{ox+di}
1	4.0 (18.2)	5.9 (26.8)	9.9 (45.0)	2.0 (5.7)	1.3 (3.6)	3.3 (9.3)
55	5.1 (19.6)	7.8 (30.2)	12.9 (49.8)	1.8 (4.1)	1.3 (3.0)	3.1 (7.1)
750	3.1 (13.0)	7.4 (30.7)	10.5 (43.7)	2.3 (5.5)	1.3 (3.0)	3.6 (8.5)
3000	4.2 (5.2)	7.0 (8.7)	11.2 (13.9)	1.8 (1.6)	1.2 (1.1)	3.0 (2.7)

Table 4
Mineral composition (% by mass) of surface soil (0–15 cm) and dust as quantified by the Rietveld refinement of synchrotron X-ray diffraction data. "×" means not detected (detection limit is about 0.3%). The values in the parentheses are standard errors of the Rietveld refinement.

Age (ky)	Anorthite	Augite	Olivine	Quartz	Calcite	Dolomite	Muscovite	Hematite	Gypsum
Soil									
1	58 (4)	21 (2)	16 (1)	5 (1)	×	×	×	×	×
55	31 (2)	9 (1)	×	13 (1)	×	×	44 (4)	4 (0)	×
750	26 (3)	×	×	26 (2)	×	×	38 (5)	11 (1)	×
3000	25 (3)	×	×	32 (2)	×	×	41 (4)	2 (0)	×
Dust									
1	59 (4)	20 (2)	8 (1)	13 (1)	×	×	×	×	×
55	43 (3)	7 (1)	×	18 (1)	×	×	31 (3)	2 (0)	×
750	20 (2)	×	×	34 (2)	3 (1)	3 (1)	37 (4)	2 (0)	1 (0)
3000	43 (3)	18 (1)	×	40 (3)	×	×	×	×	×

the 55-ky site (2%) and its concentration increased to a maximum at the 750-ky site (10%) and then decreased to 2% at the 3000-ky site.

The contemporary dust samples collected at the four sites contained similar types of minerals as the surface soils, and the mineralogical composition of the dust varied greatly across the sites (Table 4). All four sites contained anorthite (20–59%) and quartz (13–40%). Augite (7–20%), olivine (8%), muscovite (31–37%) and hematite (2%) appeared in the dust only at some of the sites (Table 4). In addition, carbonate and sulfate minerals, including 3% calcite, 3% dolomite and 1% gypsum, were detected in the dust only at the 750-ky site.

3.4. Phosphorus speciation

3.4.1. Phosphorus reference spectra

The P K-edge XANES spectra of the P standards differed in their pre-edges, whiteline positions and post-edges. The two Ca-P standards (i.e., HAP, and $Ca(H_2PO_4)_2{\cdot}H_2O$) had strong shoulders at 2154.87 eV and two pronounced peaks in the post-edge region (Fig. 4a). These features were stronger for HAP than for $Ca(H_2PO_4)_2{\cdot}H_2O$ because more Ca ions are bound to each phosphate anion in HAP. The Fe-P standard had a pre-edge feature at 2148.20 eV and its whiteline shifted to higher energy relative to those of the Ca-P standards (Fig. 4a). The Al-P standard had a similar whiteline position and slightly different post-edges compared to the Fe-P standard, but with no pre-edge features (Fig. 4a). The spectrum of sodium phytate, representing soil P_o, had a markedly broad whiteline peak, and the peak position was located between those of Ca-P and Fe- and Al-P (Fig. 4a). The features of these standards are consistent with those reported previously (Giguet-Covex et al., 2013; Hesterberg et al., 1999; Prietzel et al., 2013). The spectrum of the Al-P standard was slightly different from that of berlinite ($AlPO_4$) used in Prietzel et al. (2013), particularly in their post-edge regions. This differ-

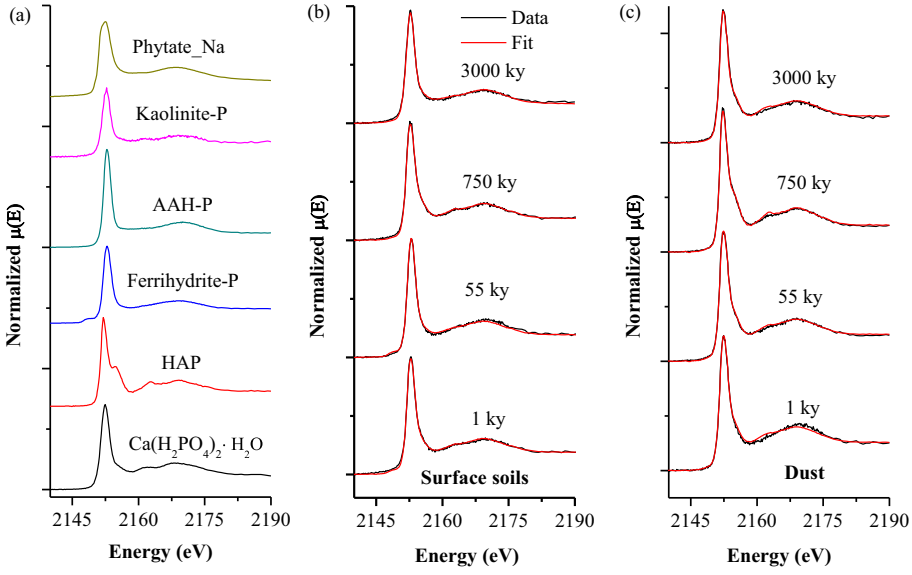

Fig. 4. The phosphorus K-edge XANES spectra of standard compounds used in the linear combination fitting (a) and comparisons of the linear combination fits and the spectra obtained from surface soil (0–15 cm, (b) and dust (c) collected along the substrate age gradient. HAP: hydroxyl apatite; Ferrihydrite-P, AAH-P and Kaolinite-P are Fe-bound and Al-bound P, represented by phosphate adsorbed on ferrihydrite, amorphous Al hydroxides (AAH), and kaolinite, respectively.

Table 5
Molar contribution (%) of each phosphorus (P) species to total P in surface soil (0–15 cm; one composite sample per site) and dust across the soil chronosequence as quantified by linear combination fitting (LCF) analysis of P K-edge XANES spectra. The standard errors in the parentheses are for the LCF analysis although the actual uncertainties for the overall XANES analysis could be lower. R factor is a measure of goodness of fit.

Age (ky)	Al-P	Fe-P	P_o	Ca-P	R factor
Soil					
1	14 (4)	47 (4)	6 (1)	33 (4)	0.00317
55	14 (3)	68 (5)	1 (1)	17 (4)	0.00357
750	30 (3)	19 (4)	12 (1)	39 (3)	0.00219
3000	47 (3)	14 (4)	23 (1)	16 (3)	0.00268
Dust					
1	0 (5)	20 (6)	25 (3)	55 (6)	0.00604
55	0 (2)	23 (1)	20 (1)	58 (3)	0.00207
750	0 (5)	20 (2)	7 (2)	74 (3)	0.00185
3000	3 (5)	9 (4)	23 (2)	66 (4)	0.00376

ence is likely due to the standard used in the present study being a sorption sample with likely some minor $AlPO_4$ precipitate, thus having less Al cations bound to each phosphate anion than in berlinite. Berlinite was unlikely to form in our soils given the weakly acidic pH conditions (Lindsay, 1979).

3.4.2. Phosphorus speciation in soils

The XANES spectra of the two younger soils, but not of the two older ones, had a subtle pre-edge (Fig. 4b). Furthermore, the whitelines of the two younger soil spectra also showed significant right shifts compared to those of the older ones (see enlarged plots in Fig. A3), suggesting higher Fe-P in the two younger soils. The spectrum of the 750-ky old soil displayed the strongest Ca-P feature (Fig. 4b), indicating that the soil contained the highest proportion of Ca-P among the four soils.

A comparison of the spectra to the fits produced using XANES LCF analysis is provided in Fig. 4b, and the fitting results are given in Table 5 and Fig. 5a. The small *R* factor values ($\ll$0.05, Table 5) indicated high goodness of fit and thus, the major P speciation of the soil samples was well represented by a combination of the five P standards. Due to the ambiguity in differentiating different Ca-P species (Kruse et al., 2015), the contributions represented by HAP and $Ca(HPO_4)_2{\cdot}H_2O$ were combined as Ca-P. Results

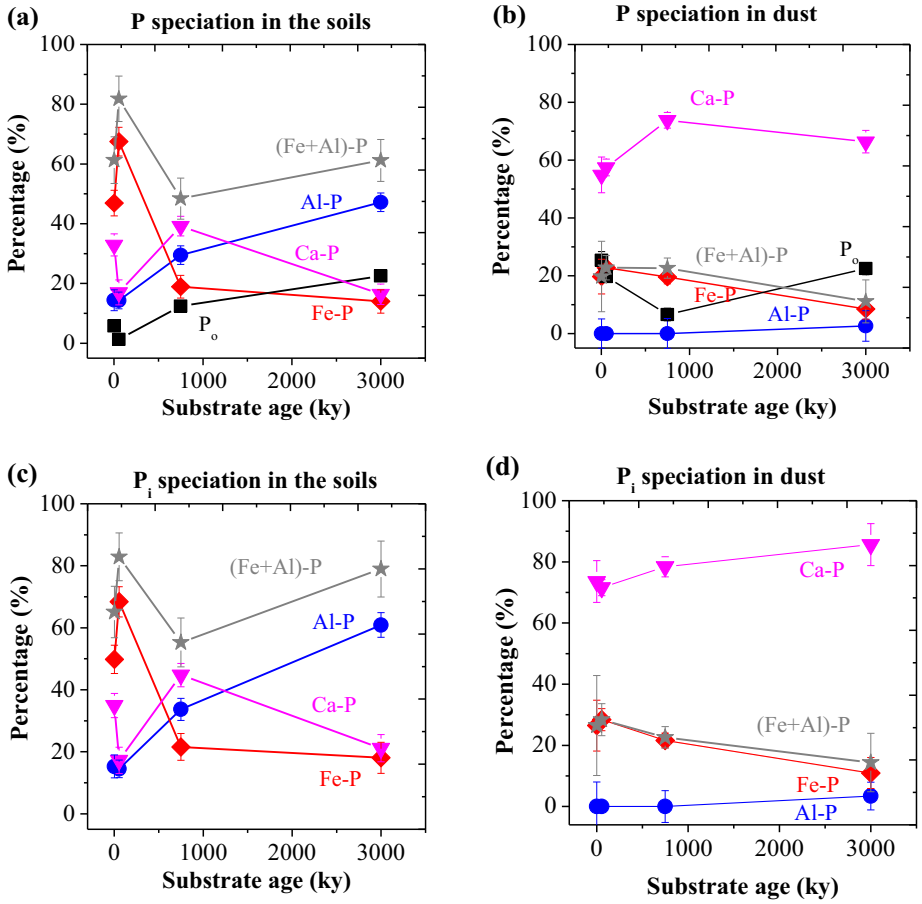

Fig. 5. The XANES-derived percentage of each phosphorus (P) species relative to total P and the percentage of each inorganic P species to the total inorganic P for soil (a, c) and dust (b, d). (Fe + Al)-P is the sum of Fe-P and Al-P. The standard deviations of the data are from the LCF fitting analysis as given in Table 5.

show that Ca-P was quite low at the youngest site, only accounting for 33% of the total P. Calcium-P decreased to 17% at the 55-ky site and then increased to 39% before it decreased again to 16% at the oldest site. The Fe-P percentage increased from 47% of the total P at the 1-ky site to 68% at the 55-ky site, and then decreased to 14–19% at the older sites. Aluminum-P monotonically increased from 30% to 47% with increasing substrate age (Fig. 5a). Together, Fe-P and Al-P (denoted as (Fe + Al)-P) contributed 48–81% of the total P, with the lowest value at the 750-ky site. Similar to Ca-P, (Fe + Al)-P did not monotonically decrease with increasing substrate age (Fig. 5a). The relative pool sizes of the Fe-P and Ca-P were in good agreement with the spectral features described above. The P_o contribution was quite low for the two younger soils (<6%), but increased to 22% at the oldest site, which are close to the concentrations determined from sequential chemical extractions in Selmants and Hart (2010). The XANES-derived P_o percentages were also similar to those determined based on NaOH-EDTA extractions that can effectively extract P_o from soils (Turner et al., 2005, Table A1). Thus, Na-phytate appears to be an adequate model organic P compound in the XANES LCF analysis of our soil samples, although some organic P compounds may be bound to Ca, Fe and Al (Prietzel et al., 2016). Excluding P_o, the Ca-P and (Fe + Al)-P, respectively, contributed 20–45% and 55–82% of the soil total inorganic P, both of which fluctuated with increasing substrate age (Fig. 5c).

3.4.3. Phosphorus speciation in dust

The spectra of the dust samples are shown in Fig. 4c. All spectra have marked Ca-P characters (i.e., the pronounced shoulder peaks and two broad peaks of the post-edge), indicating dominance of Ca-P. The XANES LCF analysis showed that the dust contained high fractions of Ca-P (Table 5 and Fig. 5b), around 55% at the two younger sites, and 79% and 65%, respectively, at the 750-ky and 3000-ky old sites (Fig. 5b). Aluminum-P was negligible and Fe-P accounted for only 10–20% of the dust inputs (Fig. 5b). The P_o contribution was quite high (20–25%) except for the dust collected at the 750-ky site, which contained about 7% P_o (Table 5 and Fig. 5b). The XANES-derived P_o proportions are slightly higher than those determined from the NaOH-EDTA extractions (8–18%, Fig. A4 of the Electronic Annex), which also show the lowest P_o proportion at the 750-ky site. Excluding P_o, Ca-P contributed 70–80% of the dust total inorganic P at all four sites (Fig. 5d).

4. DISCUSSION

4.1. Aeolian dust mass contributions to soils

Quartz is absent in basalt and basalt-derived soils, but the basalt-derived soils at all four sites in our study contained significant amounts of quartz (5–32%; Table 4), demonstrating a considerable contribution of aeolian dust (Kennedy et al., 1998; Kurtz et al., 2001; Rasmussen et al., 2017). This is supported by the increasing quartz concentration along the chronosequence, which indicates an increasing contribution of dust to soil mass with increasing substrate age (Kennedy et al., 1998). Our estimates of dust mass contributions to soils on the San Francisco Volcanic Field, using the method of Rasmussen et al. (2017) and an average quartz concentration in topsoil of the Coloradto Plateau (31.4%), yield higher dust contributions (17–103%) than previous estimates based on the strontium isotope analysis (Coble et al., 2015; Table 1). The discrepancy could be caused by possible deviations in the quartz concentrations in the dust from the average Colorado Plateau quartz concentration value used in these estimates, or weathering and biological cycling might have altered the soil Sr isotope composition (Coble et al., 2015). An alternative method to estimate dust input using muscovite mica, which is absent in underlying parent materials and rarely forms pedogenically (Dymond et al., 1974), is proved unhelpful, because muscovite concentrations did not change monotonically with increasing substrate age, suggesting the muscovite concentration in dust varies more than that of quartz.

The abundance of unweathered minerals such as anorthite and augite and the generally low CIA values suggest that the dust in our study was generated from weakly weathered dryland soils. However, the varied mineralogy of the dust samples across the four sites, particularly the presence of carbonate and sulfate minerals in the dust at the 750-ky site, suggests different dust sources across the chronosequence. The 750-ky site is located at the edge of the San Francisco Volcanic Field (Fig. A1), which might be a reason for deposition of dust with different composition. The similarity in mineralogy between the dust and the soil at each site suggests some local sources, which is typical of continental dust (Kennedy et al., 1998). However, the presence of quartz and mica in the soil indicates that at least some dust was generated from distant sources, given the absence of these minerals on nearby basaltic soils.

4.2. Soil properties and effects of aeolian dust inputs

Pedogenesis in humid climates is strongly influenced by chemical weathering, involving acidification, weathering of primary minerals, loss of soluble elements, accumulation of Si-poor secondary clay minerals, enrichment of clay and sesquioxides (mainly Fe and Al oxides), and translocation of P-bearing compounds (Muhs, 2001; Nieuwenhuyse and Van Breemen, 1997; Vitousek et al., 1997; Werner et al., 2017). As a result of these processes, solum thickness, clay content, Fe_{ox+di} and the total Fe and Al concentrations all increase, while SiO_2, Na_2O, MgO and CaO concentrations decrease (Muhs, 2001; Nieuwenhuyse and van Breemen, 1997; Vitousek et al., 1997). Pedogenic processes in a cool, semi-arid ecosystem share some of the processes as those found in humid ecosystems but they occur at much lower rates (Beal et al., 2016; Harden, 1988b; Jahn and Stahr, 1996; McFadden et al., 1986; Pavich et al., 1986; Vaughan et al., 2011). Carbonates may not accumulate in surface soils of a cool, semi-arid ecosystem despite limited leaching, as shown in the present study and others (Frey et al., 2013; Harden, 1982; Vaughan et al., 2018).

In the present study, total Fe and Al both decreased while both SiO_2 concentration and the K_2O/TiO_2 ratio

increased with increasing substrate age (Table 2 and Fig. 2). The decreases in total Fe and Al are ascribed to the increasing soil mass contribution of aeolian dust that contained lower Fe and Al than the basalt-derived soils, except at the oldest site (Table 2). The substantial accumulation of quartz and muscovite, the major K-bearing mineral, from dust inputs likely contributes to the increasing SiO_2 and K_2O/TiO_2 (Table 2 and Fig. 2). It also leads to the increasing K/Na (Table 1) and SiO_2/Al_2O_3 ratios (Fig. 2d) with increasing substrate age, the weathering indices that are expected to decrease with increasing weathering (Birkeland, 1999; Muhs, 2001; Ruxton, 1968; Selmants and Hart, 2010). In fact, assuming quartz weathering in these soils is negligible considering the semi-arid climate, the content ratio of remaining Si-bearing minerals to Al_2O_3 indeed decreased with increasing substrate age (Fig. 2d, and the calculations of the ratios are described in the figure title). Although the increase of CIA and the decrease of Al_{ox} across the soil chronosequence () are consistent with the soil development, their actual values can be altered by dust inputs (McLennan, 1993; Nesbitt and Young, 1982). The decrease in Al_{ox} is because basalt weathered quickly to non-crystalline Al-bearing minerals (e.g., imogolite and allophane) that transform to well-crystallized minerals during weathering (Selmants and Hart, 2010).

Dust inputs contribute to the decrease in soil Fe_{ox+di} and Fe_{ox} with increasing substrate age (Fig. 3e and f) because dust contains substantially lower Fe_{ox+di} and Fe_{ox} than the soil (Table 3 and Fig. 3). Crystallization of Fe_{ox} into Fe_{di} is another important reason for the decrease of Fe_{ox}, which is favored in dry environments (Chorover et al., 2004; Rasmussen et al., 2010) (Table 4). Considering the lower weathering intensity in the semi-arid environment, the initial increase of Fe_{ox} is more rapid than those in the Hawaiian chronosequence (Mikutta et al., 2009), which can be ascribed to the fast weathering of porous scoria in Arizona as opposed to lava in Hawaii (Vitousek et al., 1997). The slower decrease of Al_{ox} than Fe_{ox} correlates with the slower decrease of total Al than total Fe (i.e., the decreasing Fe_2O_3/Al_2O_3 ratio in Fig. 2d), which can be ascribed to the inputs of dust containing higher Al than Fe concentration (Table 2).

The input of alkaline dust increases soil pH, particularly when the dust contains carbonates as at our 750-ky site. Assuming that the contemporary dust composition represents the composition of dust deposited during the lifespan of the substrate surface, a mass balance calculation for the 750-ky site shows that carbonates (3% calcite + 3% dolomite = 6% total) from aeolian dust input, if not weathered in the soil, would contribute 3.2 to 4.9% of the soil mass, based on dust mass contributions of 54% and 82%, respectively, sufficient to explain the abnormally high soil pH. Although we did not detect carbonates in dust at the other sites, we postulate that dust inputs have also increased soil pH at those sites, because the dust materials must be alkaline as indicated by the dominance of Ca-P (Fig. 5b and d). In addition, our analysis is based on contemporary dust samples, but dust in the past might have been richer in carbonates, because dryland soils are typically predominant dust sources (Hou et al., 2018; Hudson-Edwards et al., 2014; Zhang et al., 2018). Overall, the magnitude of the dust-related pH increase depends on dust composition (e.g., carbonate content), flux, and the time exposed to dust deposition, leading to variation in soil pH with increasing substrate age (Table 1).

The present study examined the top 15-cm of soils (A horizon) instead of the entire soil profiles. However, the leaching of the major mobile elements (e.g., Na, Mg and Ca) from the surface soil is similar to leaching from the entire soil profiles examined in previous studies (Harden, 1988a). More importantly, the surface soil is more strongly influenced by dust than deeper parts of the profile (Rasmussen et al., 2017), and the dust incorporated into the surface soil is more modern than dust incorporated into the deeper soil (Reheis et al., 1995). Both of these conditions suggest that the changes we observed in soil P pools and other soil properties due to exogenous dust inputs over time in surface soils are representative of impacts throughout the soil profile, although they are likely expressed maximally in surface horizons.

4.3. Soil P speciation and effects of aeolian dust inputs

In our study, dust contained abundant Ca-P, consistent with its alkaline and calcareous nature and in agreement with previous studies of dust generated from drylands (Hou et al., 2018; Hudson-Edwards et al., 2014; Zhang et al., 2018). However, the dust at three sites also contained considerable P_o (20–25%), despite P_o in dryland soils typically constituting only about 10% of the total P (Cross and Schlesinger, 2001; Neff et al., 2006; Selmants and Hart, 2010; Turner et al., 2003). This suggests that dust in our study included pollen, microorganisms, and other organic particulates during dust transport and collection (Hou et al., 2018; Longo et al., 2014; Shen et al., 2007).

According to the Walker and Syers model, the Ca-P pool declines during long-term pedogenesis due to weathering and acidification, while the relative proportion of the (Fe + Al)-P pool increases as P becomes sorbed and occluded within secondary minerals. However, our XANES results show fluctuating Ca-P and (Fe + Al)-P percentages with substrate age, with relatively high proportions of Ca-P (16–39% of total P) in soils of the two oldest sites. We ascribe this surprising finding to the massive aeolian dust contributions (54–100%) on the oldest soils, because the dust contained abundant Ca-P. Furthermore, dust deposition increased soil pH, increasing the stability of Ca-P in soil and slowing chemical weathering, rates of which are already relatively slow in the semi-arid environment. The fluctuation of Ca-P and (Fe + Al)-P across the soil chronosequence can thus be ascribed to spatial and temporal variation in dust flux and composition.

The modern dust collected in this study might differ from dust deposited during the long history of soil development. The three older sites experienced glacial-interglacial cycles and were therefore presumably exposed to higher dust loadings than the youngest site during the Pleistocene glacial maxima (Goudie and Middleton, 2001; Tsoar and Pye, 1987). In addition, the older sites might have received

more volcanic ash than the younger ones as they experienced more eruptions during development of the San Francisco Volcanic Field (Tanaka et al., 1986). Nevertheless, Ca-P is the main P species in unweathered volcanic and glacial dust materials, and the depostion of these aeolian materials would have imposed similar, or even stronger, impacts as the contemporary dust generated from drylands. The cool, wet glacial periods (Anderson et al., 2000a, 2000b) would be expected to accelerate the weathering of dust, residual soil and parent material. However, the overall effect of dust inputs and changing climate during soil development at those older sites is to limit soil acidification, as indicated by the relatively high pH values (Table 1).

4.4. Effects of weathering intensity on dust perturbation of P transformation patterns

In addition to dust composition and flux, the intensity of weathering in an ecosystem affects how strongly dust deposition perturbs P transformation during long-term pedogenesis. The influence of dust deposition on P transformations observed in our study is likely to be reduced in humid ecosystems, where intense weathering leads to rapid dissolution of dust and conversion of Ca-P to (Fe + Al)-P and P_o (Abouchami et al., 2013; Eger et al., 2013a). Thus, dust inputs in a humid ecosystem likely manifest as increasing (Fe + Al)-P and P_o concentrations, rather than an accumulation of Ca-P. The perturbation of dust deposition on P transformations in a semi-arid or humid ecosystem can be regarded as a function of the ratio (r) of the net dust flux (dust flux minus loss of dust via physical erosion) to the weathering rate (Fig. 6). The ratio is similar, but not identical, to the dust supply index (DSI) proposed recently to assess the relative importance of dust and bedrock nutrient supply to soils (Arvin et al., 2017). Low and high r values are typical of humid and semi-arid ecosystems, respectively. Soil chronosequences in humid ecosystems, such as those in the Hawaiian archipelago and New Zealand (Chadwick et al., 1999; Eger et al., 2013a) with the dust flux comparable or higher than at the SAGA sites (Eger et al., 2013a; Vitousek et al., 1997), may be useful for testing this model.

4.5. Comparison between XANES analysis and sequential chemical extractions

Our study demonstrates the advantages of using P K-edge XANES spectroscopy for examining soil P transformations during soil development, and suggests that traditional sequential chemical extraction techniques may provide misleading information. For examine, in contrast to the XANES results in the present study, Selmants and Hart (2010) showed that P transformations at these SAGA sites followed the Walker and Syers model based on the modified Hedley sequential chemical extractions, with the Ca-P pool decreasing monotonically with increasing substate age (Fig. 1b). The observed consistency with the Walker and Syers model in Selmants and Hart (2010) is caused by marked overestimation of the soil Ca-P percentages at the two younger sites by sequential extraction (61–65% by Hedley fractionation versus 16–37% by XANES

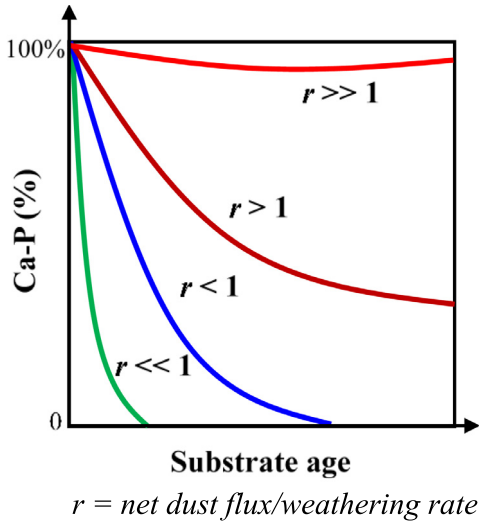

Fig. 6. A conceptual model describing how the relative magnitude (r) of the net dust flux to the dust weathering rate affects the soil Ca-P proportions during long-term soil development in semi-arid or humid environments. This model assumes that (1) deposited dust is alkaline (less weathered than soil) as aeolian dust are usually generated from drylands although not always (Wagenbach and Geis, 1989), (2) that deposited dust remains the same in chemical composition and mineralogy during soil development, and (3) that climate conditions do not change. In reality, these factors fluctuate more or less, such as during the Quaternary period. Thus, fluctuations of the Ca-P proportions with ecosystem development are expected, as shown in the present study; but overall, the Ca-P proportions are elevated by dust input.

spectroscopy). An overestimation of Ca-P by extraction was also observed in a recent study characterizing P speciation in basalt-derived soils in the Hawaii Archipelago (Helfenstein et al., 2018). Such overestimation coincidentally led to the monotonic decrease in Ca-P and thus concealed the effects of dust inputs on the pattern of P transformations. The discrepancy highlights the advantage of using direct P speciation approaches to examine P dynamics in soils. Our results suggest the possibility that previous studies that used sequential fractionations to examine chronosequences might also have overestimated the Ca-P pool (Crews et al., 1995; Lichter, 1998; Parfitt et al., 2005; Prietzel et al., 2013; Turner and Laliberté, 2015; Vitousek and Farrington, 1997; Walker and Syers, 1976). Further studies are required to examine P pools in soils developed on contrasting parent materials to determine whether the overestimation of Ca-P by sequential fractionaition is widespread.

4.6. Conclusions

Understanding P transformations during ecosystem development has important implications for evaluating contemporary cycling of P and other nutrients, and for determining how changes in P availability might affect diverse ecosystem processes. Aeolian dust inputs are ubiquitous and provide an additional P source to ecosystems, even when P supply from bedrock is substantial (Aciego

et al., 2017; Arvin et al., 2017). However, it remains poorly understood how dust inputs affect P transformation during ecosystem development. In this study, using P K-edge XANES spectroscopy, a direct P speciation approach, we found that dust inputs strongly altered the P transformation pattern by increasing Ca-P and decreasing (Fe + Al)-P proportions in older soils of a 3000-ky semi-arid soil chronosequence derived from a volcanic substrate. The impact of dust input on P transformations is concealed by using sequential chemical extractions that quantify P pools of the Walker and Syers model.

We propose a new conceptual model describing the degree of dust impact on pedogenesis as a function of the relative magnitude of net dust inputs and soil weathering rates. Our model suggests that P transformations in semi-arid ecosystems, which have weak weathering intensities that preserve accumulated dust and high dust input rates, can be strongly influenced by aeolian dust inputs. In humid ecosystems that have intense weathering, dust materials are rapidly altered, and thus the influence of aeolian inputs on pedogenesis are relatively weak. Dust inputs in semi-arid ecosystems can alter and diversify P speciation, potentially affecting plant nutrient acquisition strategies and the coupling to C and N cycles (Ceulemans et al., 2017; Delgado-Baquerizo et al., 2013; Lang et al., 2017; Zemunik et al., 2015). Our work suggests that dust input rates and composition, and weathering intensity of an ecosystem, must be considered for developing integrated climate-biogeochemical models with predictive power. Our results are particularly important considering that semi-arid ecosystems occupy ~15% of the Earth's land surface (Archibold, 1995) and that dust inputs are projected to intensify globally with increased aridity and intensification of land-uses worldwide (Aciego et al., 2017; Arvin et al., 2017; Dai, 2013; Neff et al., 2008). Overall, this study provides a foundation for understanding how dust inputs influence P dynamics in contrasting ecosystems.

ACKNOWLEDGMENTS

This work was funded by the U.S. National Science Foundation Faculty Early Career Development Program (EAR-1752903). Partial support was from the Wyoming Agricultural Experimental Station Competitive Research Grant and the Roy J. Shlemon Center for Quaternary Studies at the University of Wyoming. S.C. Hart was supported, in part, by a U.S. National Science Foundation grant, through the Southern Sierra Critical Zone Observatory (EAR-1331939). We thank P.C. Selmants and A.A. Coble for collecting and providing the dust and soil samples used in this study. Soil and dust samples were collected during research funded by the Mission Research Program at the Northern Arizona University School of Forestry (McIntire-Stennis/AZ Bureau of Forestry). The authors are grateful to the beamline scientists Qunfeng Xiao and Aimee Maclennan at the Canadian Light Source for providing technical support during P K-edge XANES data collection. We also thank Ph.D. graduate student Peng Yang in Soil and Environmental Biogeochemistry Group at the University of Wyoming for his assistance in the quantitative XRD analysis. A portion of the research described in this work was performed at the Canadian Light Source, which is supported by the Natural Sciences and Engineering Research Council of Canada, the National Research Council Canada, the Canadian Institutes of Health Research, the Province of Saskatchewan, Western Economic Diversification Canada, and the University of Saskatchewan. Use of the Advanced Photon Source, Argonne National Laboratory, supported by U.S. DOE–BES under Contract DE-AC02-06CH11357.

APPENDIX A. SUPPLEMENTARY MATERIAL

Supplementary data to this article can be found online at https://doi.org/10.1016/j.gca.2018.12.017.

REFERENCES

Abouchami W., Näthe K., Kumar A., Galer S. J., Jochum K. P., Williams E., Horbe A. M., Rosa J. W., Balsam W. and Adams D. (2013) Geochemical and isotopic characterization of the Bodélé Depression dust source and implications for transatlantic dust transport to the Amazon Basin. *Earth Planet. Sci. Lett.* **380**, 112–123.

Aciego S. M., Riebe C. S., Hart S. C., Blakowski M. A., Carey C. J., Aarons S. M., Dove N. C., Botthoff J. K., Sims K. W. W. and Aronson E. L. (2017) Dust outpaces bedrock in nutrient supply to montane forest ecosystems. *Nat. Commun.* **8**, 14800.

Ajiboye B., Akinremi O. O., Hu Y. and Jürgensen A. (2008) XANES speciation of phosphorus in organically amended and fertilized vertisol and mollisol. *Soil Sci. Soc. Am. J.* **72**, 1256–1262.

Almond P., Moar N. and Lian O. (2001) Reinterpretation of the glacial chronology of South Westland, New Zealand. N.Z. *J. Geol. Geophys.* **44**, 1–15.

Anderson R. S., Betancourt J. L., Mead J. I., Hevly R. H. and Adam D. P. (2000a) Middle- and late-Wisconsin paleobotanic and paleoclimatic records from the southern Colorado Plateau, USA. *Palaeogeogr. Palaeoclimatol. Palaeoecol.* **155**, 31–57.

Anderson R. S., Betancourt J. L., Mead J. I., Hevly R. H. and Adam D. P. (2000b) Middle- and late-Wisconsin paleobotanic and paleoclimatic records from the southern Colorado Plateau, USA. *Palaeogeogr. Palaeoclimatol. Palaeoecol.* **155**, 31–57.

Archibold O. W. (1995) *Ecology of World Vegetation*. Chapman and Hall, London, UK.

Arvin L. J., Riebe C. S., Aciego S. M. and Blakowski M. A. (2017) Global patterns of dust and bedrock nutrient supply to montane ecosystems. *Sci. Adv.* **3**.

Barbanti A., Bergamini M., Frascari F., Miserocchi S. and Rosso G. (1994) Critical aspects of sedimentary phosphorus chemical fractionation. *J. Environ. Qual.* **23**, 1093–1102.

Beal L. K., Huber D. P., Godsey S. E., Nawotniak S. K. and Lohse K. A. (2016) Controls on ecohydrologic properties in desert ecosystems: Differences in soil age and volcanic morphology. *Geoderma* **271**, 32–41.

Birkeland P. W. (1999) *Soils and Geomorphology*, third ed. Oxford University Press, New York, USA.

Ceulemans T., Bodé S., Bollyn J., Harpole S., Coorevits K., Peeters G., Van Acker K., Smolders E., Boeckx P. and Honnay O. (2017) Phosphorus resource partitioning shapes phosphorus acquisition and plant species abundance in grasslands. *Nat. Plants* **3**, 16224.

Chadwick O. A., Derry L. A., Vitousek P. M., Huebert B. J. and Hedin L. O. (1999) Changing sources of nutrients during four million years of ecosystem development. *Nature* **397**, 491–497.

Chipera S. J. and Bish D. L. (2013) Fitting full X-ray diffraction patterns for quantitative analysis: a method for readily quantifying crystalline and disordered phases. *Adv. Mater. Phys. Chem.* **3**, 30340.

Chorover J., Amistadi M. K. and Chadwick O. A. (2004) Surface charge evolution of mineral-organic complexes during pedogenesis in Hawaiian basalt. *Geochim. Cosmochim. Acta* **68**, 4859–4876.

Coble A. A. and Hart S. C. (2013) The significance of atmospheric nutrient inputs and canopy interception of precipitation during ecosystem development in piñon–juniper woodlands of the southwestern USA. *J. Arid Environ.* **98**, 79–87.

Coble A. A. and Hart S. C. (2016) No evidence of resource limitation to aboveground growth of blue grama (Bouteloua gracilis) on 1 ky-old semi-arid substrate. *Biogeochemistry* **131**, 243–251.

Coble A. A., Hart S. C., Ketterer M. E., Newman G. S. and Kowler A. L. (2015) Strontium source and depth of uptake shifts with substrate age in semiarid ecosystems. *J. Geophys. Res. G: Biogeosci.* **120**, 1069–1077.

Condron L. M. and Newman S. (2011) Revisiting the fundamentals of phosphorus fractionation of sediments and soils. *J. Soils Sedim.* **11**, 830–840.

Crews T. E., Kitayama K., Fownes J. H., Riley R. H., Herbert D. A., Mueller-Dombois D. and Vitousek P. M. (1995) Changes in soil phosphorus fractions and ecosystem dynamics across a long chronosequence in Hawaii. *Ecology* **76**, 1407–1424.

Cross A. F. and Schlesinger W. H. (2001) Biological and geochemical controls on phosphorus fractions in semiarid soils. *Biogeochemistry* **52**, 155–172.

da Silva A. L., Hotza D. and Castro R. H. R. (2017) Surface energy effects on the stability of anatase and rutile nanocrystals: a predictive diagram for Nb_2O_5-doped-TiO_2. *Appl. Surf. Sci.* **393**, 103–109.

Dahlgren R. A., Boettinger J. L., Huntington G. L. and Amundson R. G. (1997) Soil development along an elevational transect in the western Sierra Nevada, California. *Geoderma* **78**, 207–236.

Dai A. (2013) Increasing drought under global warming in observations and models. *Nat. Clim. Change* **3**, 52–58.

Delgado-Baquerizo M., Maestre F. T. and Gallardo A., et al. (2013) Decoupling of soil nutrient cycles as a function of aridity in global drylands. *Nature* **502**, 672–676.

Dymond J., Biscaye P. E. and Rex R. W. (1974) Eolian origin of mica in Hawaiian soils. *Geol. Soc. Am. Bull.* **85**, 37–40.

Eger A., Almond P. C. and Condron L. M. (2012) Upbuilding pedogenesis under active loess deposition in a super-humid, temperate climate — quantification of deposition rates, soil chemistry and pedogenic thresholds. *Geoderma* **189–190**, 491–501.

Eger A., Almond P. C. and Condron L. M. (2013a) Phosphorus fertilization by active dust deposition in a super-humid, temperate environment—soil phosphorus fractionation and accession processes. *Global Biogeochem. Cycl.* **27**, 108–118.

Eger A., Almond P. C., Wells A. and Condron L. M. (2013b) Quantifying ecosystem rejuvenation: foliar nutrient concentrations and vegetation communities across a dust gradient and a chronosequence. *Plant Soil* **367**, 93–109.

Elser J. J., Bracken M. E., Cleland E. E., Gruner D. S., Harpole W. S., Hillebrand H., Ngai J. T., Seabloom E. W., Shurin J. B. and Smith J. E. (2007) Global analysis of nitrogen and phosphorus limitation of primary producers in freshwater, marine and terrestrial ecosystems. *Ecol. Lett.* **10**, 1135–1142.

Frey H. M., Szramek K. J., Manon M. R. and Kissane M. T. (2013) Slow chemical weathering in a semiarid climate: changes in the mineralogy and geochemistry of subaerial lava flows in the Deschutes River Basin, central Oregon. *Chem. Geol.* **347**, 135–152.

Giguet-Covex C., Poulenard J., Chalmin E., Arnaud F., Rivard C., Jenny J. P. and Dorioz J. M. (2013) XANES spectroscopy as a tool to trace phosphorus transformation during soil genesis and mountain ecosystem development from lake sediments. *Geochim. Cosmochim. Acta* **118**, 129–147.

Goudie A. S. and Middleton N. J. (2001) Saharan dust storms: nature and consequences. *Earth Sci. Rev.* **56**, 179–204.

Gu C., Wang Z., Kubicki J. D., Wang X. and Zhu M. (2016) X-ray absorption spectroscopic quantification and speciation modeling of sulfate adsorption on ferrihydrite surfaces. *Environ. Sci. Technol.* **50**, 8067–8076.

Hammersley, A.P., 1998. ESRF Internal Report, ESRF98HA01T, FIT2D V9.129 Reference Manual V3.1.

Harden J. W. (1982) A quantitative index of soil development from field descriptions: examples from a chronosequence in central California. *Geoderma* **28**, 1–28.

Harden J. W. (1988a) Genetic interpretations of elemental and chemical differences in a soil chronosequence, California. *Geoderma* **43**, 179–193.

Harden J. W. J. G. (1988b) Genetic interpretations of elemental and chemical differences in a soil chronosequence, California. *Geoderma* **43**, 179–193.

Heckman K. and Rasmussen C. (2011) Lithologic controls on regolith weathering and mass flux in forested ecosystems of the southwestern USA. *Geoderma* **164**, 99–111.

Helfenstein J., Tamburini F., von Sperber C., Massey M. S., Pistocchi C., Chadwick O. A., Vitousek P. M., Kretzschmar R. and Frossard E. (2018) Combining spectroscopic and isotopic techniques gives a dynamic view of phosphorus cycling in soil. *Nat. Commun.* **9**, 3226.

Hesterberg D., Zhou W., Hutchison K. J., Beauchemin S. and Sayers D. E. (1999) XAFS study of adsorbed and mineral forms of phosphate. *J. Synchrotron Radiat.* **6**, 636–638.

Hou E., Wen D., Kuang Y., Cong J., Chen C., He X., Heenan M., Lu H. and Zhang Y. (2018) Soil pH predominantly controls the forms of organic phosphorus in topsoils under natural broad-leaved forests along a 2500 km latitudinal gradient. *Geoderma* **315**, 65–74.

Houhou J., Lartiges B. S., Hofmann A., Frappier G., Ghanbaja J. and Temgoua A. (2009) Phosphate dynamics in an urban sewer: a case study of Nancy, France. *Water Res.* **43**, 1088–1100.

Hubbard C. R. and Snyder R. L. (1988) RIR – measurement and use in quantitative XRD. *Powder Diffr.* **3**, 74–77.

Hudson-Edwards K. A., Bristow C. S., Cibin G., Mason G. and Peacock C. L. (2014) Solid-phase phosphorus speciation in Saharan Bodélé Depression dusts and source sediments. *Chem. Geol.* **384**, 16–26.

Jahn R. and Stahr K. (1996) Development of soils and site qualities on basic volcanoclastics with special reference to the semiarid environment of Lanzarote, Canary Islands, Spain. *Rev. Mex. Cienc. Geol.* **13**, 104–112.

Kar G., Hundal L. S., Schoenau J. J. and Peak D. (2011) Direct chemical speciation of P in sequential chemical extraction residues using P K-edge X-ray absorption near-edge structure spectroscopy. *Soil Sci.* **176**, 589–595.

Kennedy M. J., Chadwick O. A., Vitousek P. M., Derry L. A. and Hendricks D. M. (1998) Changing sources of base cations during ecosystem development, Hawaiian Islands. *Geology* **26**, 1015–1018.

Kizewski F., Liu Y.-T., Morris A. and Hesterberg D. (2011) Spectroscopic approaches for phosphorus speciation in soils and other environmental systems. *J. Environ. Qual.* **40**, 751–766.

Kruse J., Abraham M., Amelung W., Baum C., Bol R., Kühn O. and Santner J. (2015) Innovative methods in soil phosphorus research: a review. *J. Plant Nutr. Soil Sci.* **178**, 43–88.

Kruse J. and Leinweber P. (2008) Phosphorus in sequentially extracted fen peat soils: A K-edge X-ray absorption near-edge structure (XANES) spectroscopy study. *J. Plant Nutr. Soil Sci.* **171**, 613–620.

Kurtz A. C., Derry L. A. and Chadwick O. A. (2001) Accretion of Asian dust to Hawaiian soils: isotopic, elemental, and mineral mass balances. *Geochim. Cosmochim. Acta* **65**, 1971–1983.

Lajtha K. and Schlesinger W. H. (1988) The biogeochemistry of phosphorus cycling and phosphorus availability along a desert soil chronosequence. *Ecology* **69**, 24–39.

Lang F., Krüger J., Amelung W., Willbold S., Frossard E., Bünemann E., Bauhus J., Nitschke R., Kandeler E. and Marhan S. (2017) Soil phosphorus supply controls P nutrition strategies of beech forest ecosystems in Central Europe. *Biogeochemistry* **136**, 5–29.

Lawrence C. R., Reynolds R. L., Ketterer M. E. and Neff J. C. (2013) Aeolian controls of soil geochemistry and weathering fluxes in high-elevation ecosystems of the Rocky Mountains, Colorado. *Geochim. Cosmochim. Acta* **107**, 27–46.

Leon-Reina L., Garcia-Mate M., Alvarez-Pinazo G., Santacruz I., Vallcorba O., De la Torre A. G. and Aranda M. A. G. (2016) Accuracy in Rietveld quantitative phase analysis: a comparative study of strictly monochromatic Mo and Cu radiations. *J. Appl. Cryst.* **49**, 722–735.

Lichter J. (1998) Rates of weathering and chemical depletion in soils across a chronosequence of Lake Michigan sand dunes. *Geoderma* **85**, 255–282.

Lindsay W. L. (1979) *Chemical Equilibria in Soils*. John Wiley and Sons Ltd..

Longo A. F., Ingall E. D., Diaz J. M., Oakes M., King L. E., Nenes A., Mihalopoulos N., Violaki K., Avila A. and Benitez-Nelson C. R. (2014) P-NEXFS analysis of aerosol phosphorus delivered to the Mediterranean Sea. *Geophys. Res. Lett.* **41**, 4043–4049.

McFadden L. D., Wells S. G. and Dohrenwend J. C. (1986) Influences of quaternary climatic changes on processes of soil development on desert loess deposits of the Cima volcanic field, California. *CATENA* **13**, 361–389.

McLennan S. M. (1993) Weathering and global denudation. *J. Geol.* **101**, 295–303.

Meixner R. E. and Singer M. J. (1985) Phosphorus fractions from a chronosequence of alluvial soils, San Joaquin Valley, California. *Soil Sci.* **139**, 37–46.

Mikutta R., Schaumann G. E., Gildemeister D., Bonneville S., Kramer M. G., Chorover J., Chadwick O. A. and Guggenberger G. (2009) Biogeochemistry of mineral–organic associations across a long-term mineralogical soil gradient (0.3–4100kyr), Hawaiian Islands. *Geochim. Cosmochim. Acta* **73**, 2034–2060.

Miller A. J., Schuur E. A. and Chadwick O. A. (2001) Redox control of phosphorus pools in Hawaiian montane forest soils. *Geoderma* **102**, 219–237.

Muhs D. R. (2001) Evolution of soils on quaternary reef terraces of Barbados, West Indies. *Quat. Res.* **56**, 66–78.

Muhs D. R. and Benedict J. B. (2006) Eolian additions to late quaternary alpine soils, Indian peaks wilderness area, Colorado front range. *Arct. Antarct. Alp. Res.* **38**, 120–130.

Neff J., Ballantyne A., Farmer G., Mahowald N., Conroy J., Landry C., Overpeck J., Painter T., Lawrence C. and Reynolds R. (2008) Increasing eolian dust deposition in the western United States linked to human activity. *Nat. Geosci.* **1**, 189–195.

Neff J. C., Reynolds R., Sanford R. L., Fernandez D. and Lamothe P. (2006) Controls of bedrock geochemistry on soil and plant nutrients in Southeastern Utah. *Ecosystems* **9**, 879–893.

Negassa W. and Leinweber P. (2009) How does the Hedley sequential phosphorus fractionation reflect impacts of land use and management on soil phosphorus: a review. *J. Plant Nutr. Soil Sci.* **172**, 305–325.

Nesbitt H. and Young G. (1982) Early proterozoic climates and plate motions inferred from major element chemistry of lutites. *Nature* **299**, 715–717.

Newman G. S. and Hart S. C. (2015) Shifting soil resource limitations and ecosystem retrogression across a three million year semi-arid substrate age gradient. *Biogeochemistry* **124**, 177–186.

Nieuwenhuyse A. and Van Breemen N. (1997) Quantitative aspects of weathering and neoformation in selected Costa Rican volcanic soils. *Soil Sci. Soc. Am. J.* **61**, 1450–1458.

Parfitt R. and Henmi T. (1982) Comparison of an oxalate-extraction methon and an infrared spectroscopic method for determining allophane in soll clays. *J. Soil Sci. Plant Nutr.* **28**, 183–190.

Parfitt R. L., Ross D. J., Coomes D. A., Richardson S. J., Smale M. C. and Dahlgren R. A. (2005) N and P in New Zealand soil chronosequences and relationships with foliar N and P. *Biogeochemistry* **75**, 305–328.

Pavich M. J., Brown L., Harden J., Klein J. and Middleton R. (1986) 10Be distribution in soils from Merced River terraces, California. *Geochim. Cosmochim. Acta* **50**, 1727–1735.

Porder S., Hilley G. E. and Chadwick O. A. (2007) Chemical weathering, mass loss, and dust inputs across a climate by time matrix in the Hawaiian Islands. *Earth Planet. Sci. Lett.* **258**, 414–427.

Prietzel J., Dümig A., Wu Y., Zhou J. and Klysubun W. (2013) Synchrotron-based P K-edge XANES spectroscopy reveals rapid changes of phosphorus speciation in the topsoil of two glacier foreland chronosequences. *Geochim. Cosmochim. Acta* **108**, 154–171.

Prietzel J., Klysubun W. and Werner F. (2016) Speciation of phosphorus in temperate zone forest soils as assessed by combined wet-chemical fractionation and XANES spectroscopy. *J. Plant Nutr. Soil Sci.* **179**, 168–185.

Rasmussen C., Dahlgren R. A. and Southard R. J. (2010) Basalt weathering and pedogenesis across an environmental gradient in the southern Cascade Range, California, USA. *Geoderma* **154**, 473–485.

Rasmussen C., McGuire L., Dhakal P. and Pelletier J. D. (2017) Coevolution of soil and topography across a semiarid cinder cone chronosequence. *CATENA* **156**, 338–352.

Ravel á. and Newville M. (2005) ATHENA, ARTEMIS, HEPHAESTUS: data analysis for X-ray absorption spectroscopy using IFEFFIT. *J. Synchrotron Radiat.* **12**, 537–541.

Reheis M. C., Goodmacher J. C., Harden J. W., McFadden L. D., Rockwell T. K., Shroba R. R., Sowers J. M. and Taylor E. M. (1995) Quaternary soils and dust deposition in southern Nevada and California. *GSA Bull.* **107**, 1003–1022.

Ruxton B. P. (1968) Measures of the degree of chemical weathering of rocks. *J. Geol.*, 518–527.

Sauer D., Schellmann G. and Stahr K. (2007) A soil chronosequence in the semi-arid environment of Patagonia (Argentina). *Catena* **71**, 382–393.

Selmants P. C. and Hart S. C. (2008) Substrate age and tree islands influence carbon and nitrogen dynamics across a retrogressive semiarid chronosequence. *Global Biogeochem. Cycl.* **22**, 1–13.

Selmants P. C. and Hart S. C. (2010) Phosphorus and soil development: does the Walker and Syers model apply to semiarid ecosystems? *Ecology* **91**, 474–484.

Shen Z., Cao J., Arimoto R., Zhang R., Jie D., Liu S. and Zhu C. (2007) Chemical composition and source characterization of spring aerosol over Horqin sand land in northeastern China. *J. Geophys. Res. Atmos.* **112**.

Shober A. L., Hesterberg D. L., Sims J. T. and Gardner S. (2006) Characterization of phosphorus species in biosolids and manures using XANES spectroscopy. *J. Environ. Qual.* **35**, 1983–1993.

Simonson R. W. (1995) Airborne dust and its significance to soils. *Geoderma* **65**, 1–43.

Sparks D. L., Page A., Helmke P., Loeppert R., Soltanpour P., Tabatabai M., Johnston C. and Sumner M. (1996) *Methods of Soil Analysis. Part 3 – Chemical Methods*. Soil Science Society of America Inc..

Tanaka K. L., Shoemaker E. M., Ulrich G. E. and Wolfe E. W. (1986) Migration of volcanism in the San Francisco volcanic field, Arizona. *Geol. Soc. Am. Bull.* **97**, 129–141.

Tsoar H. and Pye K. (1987) Dust transport and the question of desert loess formation. *Sedimentology* **34**, 139–153.

Turner B. L., Cade-Menun B. J., Condron L. M. and Newman S. (2005) Extraction of soil organic phosphorus. *Talanta* **66**, 294–306.

Turner B. L., Cade-Menun B. J. and Westermann D. T. (2003) Organic phosphorus composition and potential bioavailability in semi-arid arable soils of the western United States. *Soil Sci. Soc. Am. J.* **67**, 1168–1179.

Turner B. L. and Laliberté E. (2015) Soil development and nutrient availability along a 2 million-year coastal dune chronosequence under species-rich mediterranean shrubland in southwestern Australia. *Ecosystems* **18**, 287–309.

Vaughan K. L., McDaniel P., Strawn D. and Blecker S. (2018) Soil evolution and mass flux of basaltic cinder cones in a cool, semi-arid climate. *Soil Sci. Soc. Am. J.*.

Vaughan K. L., McDaniel P. A. and Phillips W. M. (2011) Episodic soil succession on basaltic lava fields in a cool, dry environment. *Soil Sci. Soc. Am. J.* **75**, 1462–1470.

Vitousek P. M., Chadwick O. A., Crews T. E., Fownes J. H., Hendricks D. M. and Herbert D. (1997) In this month's issue: soil and ecosystem development across the Hawaiian Islands. *GSA Today* **7**.

Vitousek P. M. and Farrington H. (1997) Nutrient limitation and soil development: experimental test of a biogeochemical theory. *Biogeochemistry* **37**, 63–75.

Wagenbach D. and Geis K. (1989) The mineral dust record in a high altitude alpine glacier (Colle Gnifetti, Swiss Alps). In *Paleoclimatology and Paleometeorology: Modern and Past Patterns of Global Atmospheric Transport* (eds. M. Leinen and M. Sarnthein). Springer, Netherlands, Dordrecht, pp. 543–564.

Walker T. W. and Syers J. K. (1976) The fate of phosphorus during pedogenesis. *Geoderma* **15**, 1–19.

Wang R., Balkanski Y., Boucher O., Ciais P., Penuelas J. and Tao S. (2015) Significant contribution of combustion-related emissions to the atmospheric phosphorus budget. *Nat. Geosci.* **8**, 48–54.

Wang X., Hu Y., Tang Y., Yang P., Feng X., Xu W. and Zhu M. (2017) Phosphate and phytate adsorption and precipitation on ferrihydrite surfaces. *Environ. Sci.: Nano* **4**, 2193–2204.

Wardle D. A., Walker L. R. and Bardgett R. D. (2004) Ecosystem properties and forest decline in contrasting long-term chronosequences. *Science* **305**, 509–513.

Webb S. M., Tebo B. M. and Bargar J. R. (2005) Structural characterization of biogenic Mn oxides produced in seawater by the marine *Bacillus* sp. strain SG-1. *Am. Mineral.* **90**, 1342–1357.

Werner F., de la Haye T. R., Spielvogel S. and Prietzel J. (2017) Small-scale spatial distribution of phosphorus fractions in soils from silicate parent material with different degree of podzolization. *Geoderma* **302**, 52–65.

Werner F. and Prietzel J. (2015) Standard protocol and quality assessment of soil phosphorus speciation by P K-edge XANES spectroscopy. *Environ. Sci. Technol.* **49**, 10521–10528.

Wu Y., Prietzel J., Zhou J., Bing H., Luo J., Yu D., Sun S., Liang J. and Sun H. (2014) Soil phosphorus bioavailability assessed by XANES and Hedley sequential fractionation technique in a glacier foreland chronosequence in Gongga Mountain, Southwestern China. *Sci. China. Earth Sci.* **57**, 1860–1868.

Yan Y., Li W., Yang J., Zheng A., Liu F., Feng X. and Sparks D. L. (2014) Mechanism of myo-inositol hexakisphosphate sorption on amorphous aluminum hydroxide: spectroscopic evidence for rapid surface precipitation. *Environ. Sci. Technol.* **48**, 6735–6742.

Zemunik G., Turner B. L., Lambers H. and Laliberté E. (2015) Diversity of plant nutrient-acquisition strategies increases during long-term ecosystem development. *Nat. Plants* **1**, 15050.

Zhang Z., Goldstein H. L., Reynolds R. L., Hu Y., Wang X. and Zhu M. (2018) Phosphorus speciation and solubility in aeolian dust deposited in the interior American west. *Environ. Sci. Technol.* **52**, 2658–2667.

Associate editor: Dominik Weiss